Single-photon interconnector composed of two individual one-dimensional nano-waveguides and a single emitter*

Xin-Qin Zhang(张新琴)[1], Xiu-Wen Xia(夏秀文)[1,2,†], Jing-Ping Xu(许静平)[2], and Ya-Ping Yang(羊亚平)[2]

[1] *Institute of Atomic and Molecular Physics and Functional Materials, School of Mathematics and Physics, Jinggangshan University, Ji'an* 343009, *China*

[2] *MOE Key Laboratory of Advanced Micro-structure Materials, School of Physics Science and Engineering, Tongji University, Shanghai* 200092, *China*

(Received 1 November 2016; revised manuscript received 16 December 2016; published online 6 April 2017)

Recently, theoretical and experimental nano-sized fundamental devices for optical circuits have been proposed at the single-photon level. The assembly of a realistic optical circuit is now a reality. In this work, we introduce a single-photon interconnector composed of two individual nanowires and an optical N-type four-level emitter that can turn the optical connection on and off optically. Because of dipole-induced transmission at the single-photon level, a single photon can travel between the two nanowires reciprocally, which guarantees its application as an all-optical interconnector.

Keywords: single-photon, nano-waveguide, optical interconnector

PACS: 42.50.Gy, 42.50.Ct **DOI:** 10.1088/1674-1056/26/5/054208

1. Introduction

Regarded as the ideal carries of quantum information, photons are naturally considered as a substitute for electrons in future information technology applications.[1,2] Controlling the scattering properties of a single photon has attracted particular interest for its applications in quantum information. In recent years, many fundamental devices for optical circuits, such as optical diodes[3–5] and transistors[6–10] at single-atom sizes or single-photon levels, have been proposed theoretically and experimentally.[11–15]

If we imagine a time in the near future when such single-photon optical elements have been fabricated, how could we assemble a realistic optical mechanism efficiently and conveniently? Although it is easy to perform single-photon propagation in a traditional optical waveguide, it remains challenging to control communication at the single-photon level.[16–21] Recently, research on single emitters coupling with nano-waveguides has received considerable attention.[2,10,22,23] These studies use light–matter interactions, which are already a fundamental topic in physics.[24] Strong light–matter interactions make the waveguide setup a promising candidate for connecting these elemental devices.[25,26]

In this paper, we describe an optically controlled interconnector composed of two individual terminated metal nanowires and an optical N-type four-level emitter, as shown in Fig. 1(a). The terminated waveguides are blocked by perfect mirrors and light will be completely reflected by the right ends. Two nanowires serve as two outside interfaces, and the N-type four-level emitter serves as the inside coupler. Each nanowire exhibits good confinement and guiding, even when its radius is reduced well below the optical wavelength. The atom has an N-type four-level structure $|s\rangle \leftrightarrow |d\rangle \leftrightarrow |g\rangle \leftrightarrow |e\rangle$ with two stable ground states, $|s\rangle$ and $|g\rangle$, and two electronic excited states, $|d\rangle$ and $|e\rangle$, as shown in Fig. 1(b). For example, we can use the sublevels $|s\rangle = |6S_{1/2}, F = 3, M = 3\rangle$, $|g\rangle = |6S_{1/2}, F = 4, M = 4\rangle$, $|d\rangle = |6P_{3/2}, F' = 4, M' = 4\rangle$, and $|e\rangle = |6P_{3/2}, F' = 5, M' = 5\rangle$ of the D_2 line of atomic caesium. We will show that the scattering properties of the system are dependent on the initial state of the atom being prepared.

For an atom prepared in state $|s\rangle$, this atom structure mediates an effective interaction between free-space photons (photons resonant with the $|s\rangle \rightarrow |d\rangle$ transition serving as gate photons) and nanowire-guided photons (photons resonant with the $|g\rangle \rightarrow |e\rangle$ transition serving as the source) through a free-space control laser that addressees the $|d\rangle \rightarrow |g\rangle$ transition. By ramping the control laser power down to zero, we store a weak gate pulse inside the atom and retrieve it at a later time by adiabatically reapplying the control beam.[9] Therefore, the atom can be prepared in states $|s\rangle$ or $|d\rangle$ optically. We will show that the atomic population in state $|g\rangle$ can open the transmission of the source pulse through the system.

*Project supported by the National Natural Science Foundation of China (Grant Nos. 11274242, 11474221, and 11574229), the Joint Fund of the National Natural Science Foundation of China and the China Academy of Engineering Physics (Grant No. U1330203), the National Key Basic Research Special Foundation of China (Grant Nos. 2011CB922203 and 2013CB632701), and the Doctor Startup Fund of the Natural Science of Jinggangshan University, China (Grant No. JZB16003).

†Corresponding author. E-mail: jgsuxxw@126.com

© 2017 Chinese Physical Society and IOP Publishing Ltd

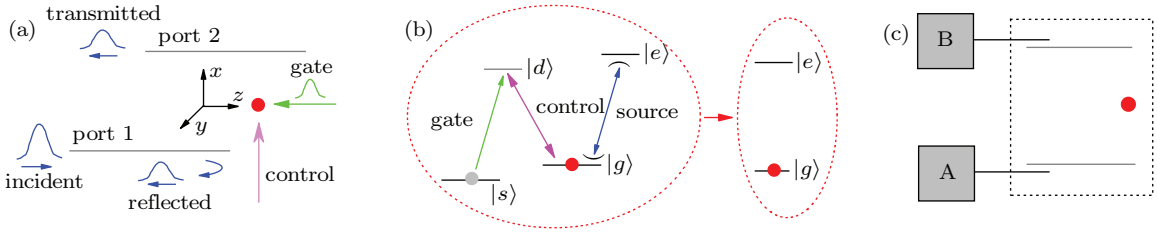


Fig. 1. (color online) (a) Atom–nanowire coupling system. Two grey terminated horizontal lines represent two individual terminal nanowires, and the small red circle denotes an N-type four-level emitter, as shown in panel (b). (c) Schematic diagram of single-photon interconnector. The dotted rectangle represents the coupling system of (a). Two optical devices A and B are connected to the interconnector through two dielectric waveguides.

Between storage and retrieval, we apply a source pulse from port 1. Here, the two nanowires only couple with the $|g\rangle \rightarrow |e\rangle$ transition at different coupling strengths k_1 and k_2. Spatial symmetry occurs when $k_1 = k_2$, whereas the system is asymmetric when $k_1 \neq k_2$. The atom–nanowire coupling strengths k_1 and k_2 are dependent on the radius of the nanowires and the position of the atom, and can be manipulated in a very large range in realistic systems according to the theoretical and experimental results.[10,22,27,28] Therefore, the source pulse will be completely reflected by the perfect mirror on the end if the atom is prepared in state $|s\rangle$.

2. Model

For an atom prepared in ground state $|g\rangle$, and only a single-photon Gaussian pulse impinging on the lower nanowire from port 1, the four-state N-type structure degenerates to a two-level system, as the source photon only interacts with the $|g\rangle \rightarrow |e\rangle$ transition, as shown in Fig. 1(b). In the frame of rotation approximation, the interaction between a single photon and a two-level emitter is modelled by the Hamiltonian[10,16,22]

$$H = H_0 + H_{\rm I}, \tag{1}$$

where

$$H_0 = \hbar\omega_{\rm at}\sigma_{ee} + \hbar\int_0^\infty {\rm d}\omega[\omega_b b^\dagger(\omega)b(\omega) + \omega_c c^\dagger(\omega)c(\omega)],$$
$$H_{\rm I} = \hbar\int_0^\infty {\rm d}\omega[g_1 b(\omega)\sigma_{eg} + g_2 c(\omega)\sigma_{eg}] + {\rm H.c.},$$

where H.c. is the complex conjugate. $\sigma_{ij} = |i\rangle\langle j|$ $(i,j = g,e)$ represent atomic operators, $\omega_{\rm at}$ is the transition frequency, and $b(\omega)$, $c(\omega)$ are the annihilation operators for mode ω in the two waveguides. g_1 and g_2 are the interaction strengths between the nanowires and the emitter, which are frequency-independent because of the narrow bandwidth of the input single-photon pulse. As we know, the interaction strength g_1 (g_2) is associated with the coupling strength k_1 (k_2), fulfilling $k_i = 2\pi\langle|g_i|^2\rangle$ $(i = 1,2)$, where angle brackets represent an angular average. Therefore, coupling strength k_i $(i = 1, 2)$ states two contradictory physical aspects: the interaction strength between the nano-waveguide and the emitter, and the energy leak rate from the atom to nano-waveguide modes. This is why k_i is named the coupling strength or leak rate.

Without loss of generality, we take the emitter position as the real-space origin ($z_{\rm at} = 0$). The two nano-waveguides are separated sufficiently that their direct coupling can be neglected. We expand the Schrodinger-picture state $|\psi(t)\rangle$ on the basis of all states with one exciton,

$$|\psi\rangle = \int_0^\infty {\rm d}\omega c_1^\omega(t)b^\dagger(\omega)|g,0_b,0_c\rangle + \int_0^\infty {\rm d}\omega c_2^\omega(t)c^\dagger(\omega)|g,0_b,0_c\rangle + c_e(t)|e,0_b,0_c\rangle, \tag{2}$$

where $|0_b\rangle$ and $|0_c\rangle$ denote the vacuum states in the lower and upper nanowires, respectively. At time $t = 0$, assume that the atom is at the ground state $|g\rangle$, and only a Gaussian single-photon wavepacket, which is defined as $c_1^\omega(0) = \left(2/\pi\Delta^2\right)^{1/4} {\rm e}^{{\rm i}(\omega-\omega_0)t_0-(\omega-\omega_0)^2/\Delta^2}$, is incident on the lower nanowire from port 1 (ω_0 and Δ are its central frequency and full width at half maximum (FWHM), fulfilling $\omega_0/\Delta \gg 1$; $t_0 = z_0/v_{\rm g}$, $-z_0$ and $v_{\rm g}$ are the position at which the peak of the pulse passes at $t = 0$ and the propagating group velocity in the nanowires, respectively).

After some algebra, we can solve the Schrodinger equation ${\rm i}\hbar\bar{\partial}|\psi\rangle/\partial t = H|\psi\rangle$ analytically. Because of the atom–nanowire interaction, some reflected field remains in the initial nanowire, while the remainder is transported to the upper nanowire or absorbed by the atom. The final shapes of the reflected and transmitted pulses are associated with the distributions of $|c_i^\omega(t\rightarrow\infty)|^2$ $(i = 1,2)$.[29] Thus, we obtain the final reflection coefficient $r(\omega) = \lim_{t\rightarrow\infty} c_1^\omega(t)/c_1^\omega(0)$ and transmission coefficient $t(\omega) = \lim_{t\rightarrow\infty} c_2^\omega(t)/c_1^\omega(0)$ as

$$r(\omega) = 1 - \frac{k_1}{\Gamma/2 - {\rm i}(\omega-\omega_{\rm at})}, \tag{3}$$

$$t(\omega) = -\frac{\sqrt{k_1 k_2}}{\Gamma/2 - {\rm i}(\omega-\omega_{\rm at})}. \tag{4}$$

Here, $\Gamma = k_1 + k_2 + \gamma_{\rm at}$ is the total decay rate due to the Purcell effect and $\gamma_{\rm at}$ is the atomic vacuum spontaneous emission rate, representing the atomic energy loss other than to waveguide modes. Therefore, $P = \Gamma/\gamma_{\rm at} - 1$ is the so-called Purcell factor, which can be manipulated in a large range from

near-zero to several hundred in present atom–photon coupling systems.[10,22] $\omega_0 - \omega_{at}$ represents the detuning between ω_0 and ω_{at}.

Note that although Eqs. (3) and (4) are obtained following a single-photon incident, they are in accordance with the results obtained from a weak monochromatic laser incident without the presence of atomic saturation nonlinearity.[10,16,22] Optical nonlinear responses can only be seen by considering the interaction of a single emitter with not only a single photon, but also multiphoton input states.[10]

Atoms can be excited by single-photon incidents. By performing a Fourier transformation on the incident single-photon function $E_{in}(\omega) = \left|c_1^{\omega}(0)\right|^2$ in the frequency domain, we obtain the wavepacket in the time domain as

$$E_{in}(t) = \frac{1}{2\pi} e^{-\frac{\Delta^2 (t-t_0)^2}{8}} e^{-i\omega_0 t}. \tag{5}$$

This shows that $E_{in}(t)$ is also a Gaussian function, with a FWHM of $t_{FWHM} = 2\sqrt{2}/\Delta$ and a central frequency of ω_0.

A long pulse in the time domain implies a small electric field intensity and a weak atom–light interaction. Therefore, the emitter shall rarely be excited at all times when $\gamma_{at}/\Delta \gg 1$. Thus, we focus on a short pulse with $\gamma_{at}/\Delta \ll 1$ and fix $\gamma_{at}/\Delta = 0.1$ throughout unless otherwise specified. Assuming that the incident wavepacket is initially far away from the emitter, we take $t_0 = 5t_{FWHM}$ throughout this paper. At this instance, there is a negligible initial interaction between the atom and the pulse.

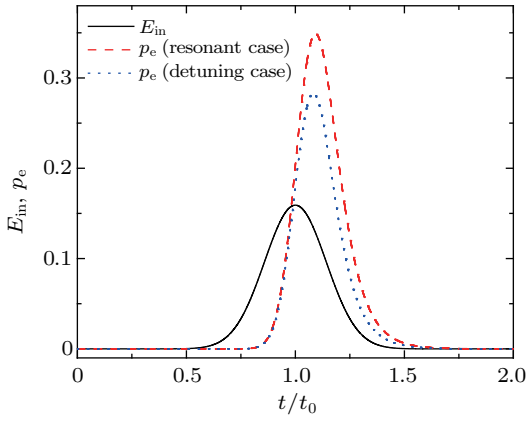


Fig. 2. (color online) Atomic excitation undergoing a Gaussian pulse incident. At $t = 0$, the peak of the incident single-photon wavepacket is located at $z = -z_0 = -v_g t_0$. The solid black line denotes the initial input single-photon wavepacket, whereas the red dash and blue dotted curves indicate the resonant case and detuning case of $|\omega_0 - \omega_{at}| = 0.5$, respectively. Other parameters are $\Delta \equiv 1$, $\gamma_{at} = 0.1$, and $k_1 = k_2 = 0.38$.

As the leading edge of the pulse reaches the emitter, the interaction effectively switches on. From this time onwards, the emitter gains an excitation amplitude, and starts to emit an outgoing wavepacket into both the lower and upper nanowaveguides. The probability of the atom being in the excited state is $p_e(t) = |c_e(t)|^2$, which can be written as

$$\begin{aligned} p_e(t) = & \sqrt{\frac{\pi}{2}} \frac{k_1}{\Delta} e^{-\frac{2(\omega_0-\omega_{at})^2}{\Delta^2} + \frac{\Gamma^2}{2\Delta^2} - \Gamma(t-t_0)} \\ & \times \left| \mathrm{erf}\left(\frac{\Delta(t-t_0)}{2} - \frac{\Gamma}{2\Delta} + i\frac{\omega_0-\omega_{at}}{\Delta} \right) \right. \\ & \left. + \mathrm{erf}\left(\frac{\Delta t_0}{2} + \frac{\Gamma}{2\Delta} - i\frac{\omega_0-\omega_{at}}{\Delta} \right) \right|^2. \end{aligned} \tag{6}$$

Here, $\mathrm{erf}(z) = \frac{2}{\sqrt{\pi}} \int_0^z e^{-t^2} dt$ is the error function extended to the complex field.[30] It is convenient to perform normalization by taking $\Delta \equiv 1$ throughout this work.

3. Results

We have plotted Fig. 2 to show the time dependence of atomic excitation undergoing a Gaussian pulse. Here, $k_1 = k_2 = 0.38$ and $\omega_0 - \omega_{at} = 0$ for the resonant case (red dash line), whereas $|\omega_0 - \omega_{at}| = 0.5$ for the detuning case (blue dotted line). It is easy to compute the Purcell factor $P = 7.6$ at this stage. The atomic population in state $|e\rangle$ is in accordance with a previous result.[22] Comparing the initial wavepacket $E_{in}(t)$ with the atomic excitations $p_e(t)$, we can see that there is a short delay in the excitation curves. This short delay causes the peak excitation to be slightly offset to the right. The maximum atomic excitation is approximately 0.35 in the resonant case, dropping to 0.28 when $|\omega_0 - \omega_{at}| = 0.5$. This decline in $p_e(t)$ in the detuning case is because the atom is easily excited when they are in tune. Furthermore, the duration of the remarkable excited atomic state is less than five times t_{FWHM}. This indicates that the atomic response for a multiphoton queue input is the same as for a single-photon input when the photons are separated by much more than five times the line-width in the real space.

Traditional dipole-induced transmission has been introduced with a monochromatic laser incident.[31,32] Here, we will introduce dipole-induced transmission at the single-photon level. From Eq. (2), we obtain the in-time probabilities of the reflected $p_r(t) = \int_0^{\infty} d\omega \left|c_1^{\omega}(t)\right|^2$ and transmitted photons $p_t(t) = \int_0^{\infty} d\omega \left|c_2^{\omega}(t)\right|^2$. As we are interested in the final probabilities for detecting the reflected and transmitted photons, we take the limits $p_r = \lim_{t\to\infty} p_r(t)$ and $p_t = \lim_{t\to\infty} p_t(t)$ to obtain the single-photon reflectivity and transmittivity long after the light–matter interaction, which can be written as

$$p_r = 1 - \frac{\sqrt{8\pi} k_1 (k_2 + \gamma_{at})}{\Gamma\Delta} \mathrm{Re}\left(w(Z)\right), \tag{7}$$

$$p_t = \frac{\sqrt{8\pi} k_1 k_2}{\Gamma\Delta} \mathrm{Re}\left(w(Z)\right). \tag{8}$$

Here, $Z = X + iY$, with $X = -(\omega_0 - \omega_{at}) t_{FWHM}/2$ and $Y = \Gamma t_{FWHM}/4$; $w(Z) = e^{-Z^2}[1 - \mathrm{erf}(-iZ)]$ is a complementary error function defined in the complex field and Re is its real

part.[30] The analytical results presented in Eqs. (7) and (8) are different from those of theoretical works[10,16,22,25,33] in the monochromatic limit, and are superior to those in a numerical study.[22]

Equations (7) and (8) are universal expressions of single-photon reflectivity and transmittivity. They can be simplified according to the value of Γ/Δ. We first investigate the monochromatic limit $\Gamma/\Delta \gg 1$, as frequently used in theoretical studies.[10,16,22,25,33] In this case, the expressions can be simplified as Lorentz functions, i.e.,

$$p_{\rm r} = \frac{(k_2 - k_1 + \gamma_{\rm at})^2/4 + (\omega_0 - \omega_{\rm at})^2}{\Gamma^2/4 + (\omega_0 - \omega_{\rm at})^2},$$
$$p_{\rm t} = \frac{k_1 k_2}{\Gamma^2/4 + (\omega_0 - \omega_{\rm at})^2}.$$

If $\Gamma/\Delta \ll 1$, they can be simplified as Gaussian functions, i.e.,

$$p_{\rm r} = 1 - \frac{\sqrt{8\pi} k_1 (k_2 + \gamma_{\rm at})}{\Gamma\Delta} {\rm e}^{-\frac{2(\omega_0-\omega_{\rm at})^2}{\Delta^2}},$$
$$p_{\rm t} = \frac{\sqrt{8\pi} k_1 k_2}{\Gamma\Delta} {\rm e}^{-\frac{2(\omega_0-\omega_{\rm at})^2}{\Delta^2}}.$$

In the regime between these limiting cases, our analytical solutions still work, i.e., they can easily cross the regime from $\Gamma/\Delta < 1$ to $\Gamma/\Delta > 1$.

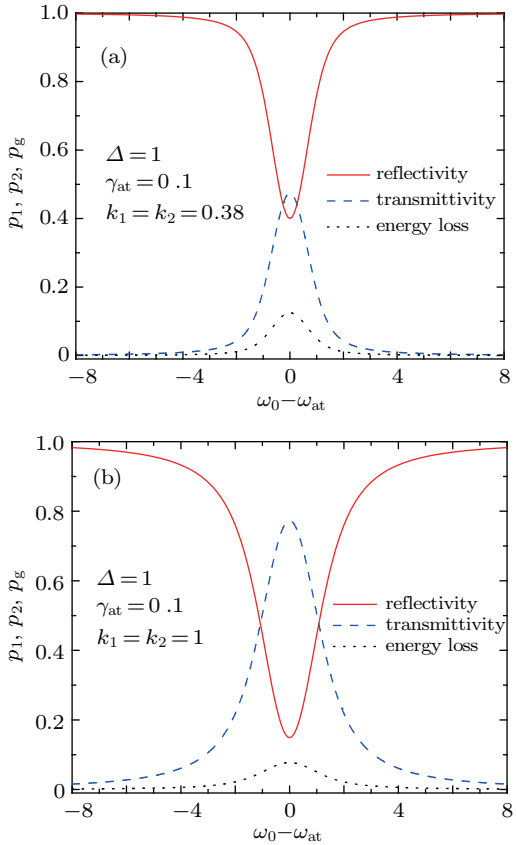


Fig. 3. (color online) Single-photon reflectivity and transmittivity. We take parameters as $\Delta \equiv 1$, $\gamma_{\rm at} = 0.1$, $k_1 = k_2 = 0.38$ in panel (a) and $k_1 = k_2 = 1.0$ in panel (b). The red solid, blue dash lines represent single-photon reflectivity and transmittivity, respectively. The energy loss rate curve is plotted as the black dotted line.

To clarify the dipole-induced transmission at the single-photon level, figure 3 shows $p_{\rm r}$ and $p_{\rm t}$ for two different Purcell factors ($P = 7.6$ and 20). We take $\Delta \equiv 1$, $\gamma_{\rm at} = 0.1$, $k_1 = k_2 = 0.38$, and show the single-photon reflectivity and transmittivity undergoing $\Gamma < \Delta$ in Fig. 3(a). When the detuning is much larger than 4.0, the incident photon rarely interacts with the atom and the photon almost remains in the initial nano-waveguide. Thus, there is almost no probability of finding transmitted photon in the upper nano-waveguide. However, when the incident photon is in tune with the atom, things change dramatically. Single-photon reflectivity drops to 0.40 and transmittivity increases to 0.47. The presence of a non-zero atomic spontaneous emission means that the summation of reflectivity and transmittivity is a little less than 100%. The single-photon reflectivity and transmittivity are also controlled by the spatial asymmetry.

Adopting the parameters in Fig. 3(a), but changing $k_1 = k_2 = 1.0$ to ensure $\Gamma > \Delta$ (strong coupling regime with $P = 20$), figure 3(b) compares the results for the case $\Gamma < \Delta$ ($P = 7.6$). We can see that single-photon reflectivity decreases to 0.15 and transmittivity increases to 0.77 when $\omega - \omega_0 = 0$. Therefore, figure 3 illustrates the effect of dipole-induced transmission at the single-photon level, and shows that a larger Purcell factor is beneficial to greater transmittivity.

Note that the energy loss rate $p_{\rm g}$ denotes the probability of the total energy emitted into vacuum modes, which is plotted in Fig. 3 as the black dotted line. This originates from the non-zero atomic spontaneous emission rate, and can be obtained using the rule of energy conservation. As $p_{\rm e}(t \to \infty) = 0$, we obtain $p_{\rm g} = 1 - p_{\rm r} - p_{\rm t}$, which gives

$$p_{\rm g} = \frac{\sqrt{8\pi} k_1 \gamma_{\rm at}}{\Gamma\Delta} {\rm Re}\left(w(Z)\right). \tag{9}$$

Here, we show how to fabricate such an atom–waveguide coupling system. Atoms can interact with optical waveguides through the evanescent field propagating on it, and the coupling strength is determined by the materials of the waveguide and the distance to the atom. Recently, an optical emitter–nanowire coupling system that exhibits a strong interaction between the atom and light has been fabricated experimentally.[10] Theoretical studies also show that the maximum Purcell factor P can vary from near-zero to several hundred with an appropriate design.[10,27,28] For example, considering a fixed 20-nm-radius silver nanowire ($\varepsilon_{\rm Ag} = -50 + 0.6{\rm i}$) embedded in the host material with index $n = 1.414$ coupled with an emitter of ^{133}Cs at a distance of 10 nm to the nanowire and an emission wavelength of 1000 nm, P is approximately 37.[22] In such a setup, it would not be difficult to fabricate our scheme using current technology and careful design.

From the above discussion, we know that if the atom decouples from the two nano-waveguides, a single photon cannot travel between the two nanowires. Only when the atom is

strongly coupled with the nanowires (see the case of $P = 20$) can a single photon be transported. We call this dipole-induced transmission at the single-photon level, and believe that this phenomenon may have implications for new quantum devices. Here, we introduce an application as an optically controlled single-photon interconnector that can turn the connection between two individual optical nano-devices on and off at the single-photon level. This is analogous to a classical switchable electronic socket and is convenient for controlling an optical circuit.

Assuming that two individual optical devices A and B communicate at the single-photon level, we must transport a single photon from A to B reciprocally. As we know, a nonlinear asymmetric system can produce non-reciprocal transport.[34–37] Here, let us examine the optical reciprocity after undergoing the single-photon incident. From Eq. (8), we can see that k_1 and k_2 appear in couples, which indicates optical reciprocity even in an asymmetric coupling environment. Optical reciprocity originates from the fact that the nonlinear response can be seen by considering the interaction of a single emitter with not only a single photon, but also multiphoton input states.[10]

Although the probability of finding a reflected photon p_r or transmitted photon p_t is less than 100%, once a reflected or transmitted photon is detected, it will be a complete single-photon wavepacket. We define the normalized reflected and transmitted spectra $R(\omega) = \left|c_1^{\omega}(0)r(\omega)\right|^2/p_\mathrm{r}$ and $T(\omega) = \left|c_1^{\omega}(0)t(\omega)\right|^2/p_\mathrm{t}$, respectively, as

$$R(\omega) = \frac{1}{p_\mathrm{r}}\left(1 - \frac{k_1(k_2+\gamma_\mathrm{at})}{\Gamma^2/4+(\omega-\omega_\mathrm{at})^2}\right) \times \left(\frac{2}{\pi\Delta^2}\right)^{1/2} \mathrm{e}^{-\frac{2(\omega-\omega_0)^2}{\Delta^2}}, \tag{10}$$

$$T(\omega) = \frac{1}{p_\mathrm{t}}\frac{k_1k_2}{\Gamma^2/4+(\omega-\omega_\mathrm{at})^2}\left(\frac{2}{\pi\Delta^2}\right)^{1/2} \mathrm{e}^{-\frac{2(\omega-\omega_0)^2}{\Delta^2}}. \tag{11}$$

To clarify the normalized reflected and transmitted spectra, we set $\Delta \equiv 1$, $\gamma_\mathrm{at} = 0.1$, $k_1 = k_2 = 1$ and plot the reflected (red solid line) and transmitted spectra (blue dash line) in Figs. 4(a) ($\omega_0 - \omega_\mathrm{at} = 0$) and (b) ($\omega_0 - \omega_\mathrm{at} = 0.5$), respectively. When the incident photon is in-tune with the atom, the transmitted spectrum has a single peak whose centre is located at ω_0. Compared with the FWHMs of the transmitted and incident wavepackets, the FWHM of the transmitted spectrum is suppressed. This indicates that, although the central frequency of the transmitted photon does not vary, its width has been compressed in the frequency domain. However, in the detuning case of $\omega_0 - \omega_\mathrm{at} = 0.5$, the transmitted photon central frequency is slightly smaller than ω_0 and slightly greater than ω_at. Therefore, the shape and central frequency of the transmitted photon can be a little different from the initial pulse. This indicates that our scheme can be used as a mild single-photon wavepacket reformer, which not only suppresses the frequency uncertainty but also shifts the central frequency to somewhere between ω_0 and ω_at.

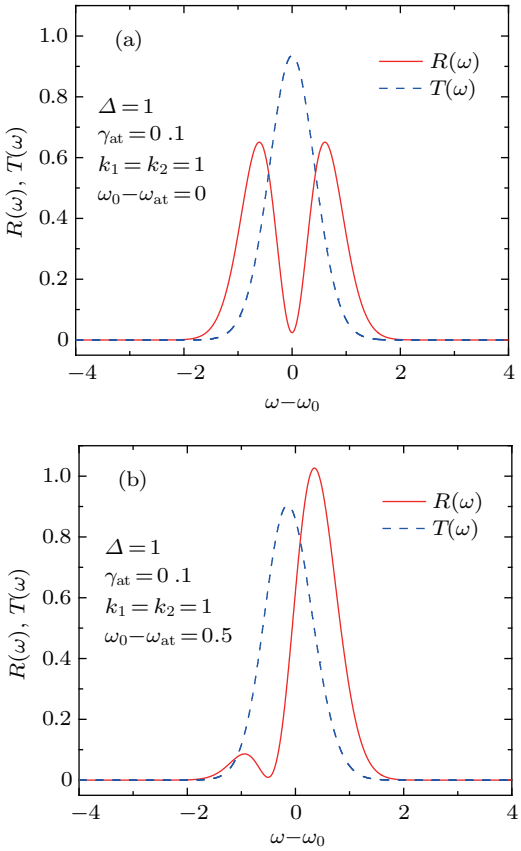


Fig. 4. (color online) Normalized reflected and transmitted photon wavepacket spectra in resonant case (a) and detuning case (b) with $\omega_0 - \omega_\mathrm{at} = 0.5$. In both (a) and (b), red solid and blue dash curves denote the reflected and transmitted wavepacket frequency spectra, respectively. We take $\Delta \equiv 1$, $\gamma_\mathrm{at} = 0.1$, and $k_1 = k_2 = 1$.

However, the reflected spectrum is much different from the transmitted one. The spectra present a traditional Rabi splitting into a symmetric doublet structure in the resonant case and into an asymmetric one in the off-resonant case. The positions of the reflected spectrum peaks are separated significantly from that of the transmitted spectrum. The holes can be attributed to destructive interference between the driving field and the re-emitted field. As the central frequency of the re-emitted field is no longer at the centre of the driving field, the destructive interference between two wavepackets with different central frequencies leads to asymmetric splitting.

Therefore, our model can be used to fabricate an all-optical single-photon interconnector similar to the schematic diagram in Fig. 1(c). Two individual dielectric waveguides extended from optical devices A and B are linked to the single-photon interconnector through nanowire–waveguide coupling. Excitations are transferred to and from the metal nanowires via the evanescently coupled, phase-matched dielectric waveguides.[10] An N-type four-level structure opti-

cal emitter is placed near the terminals of the two individual nanowires, which are sufficiently separated to ignore their direct coupling. If the atom is initially prepared in state $|s\rangle$, the decoupled system blocks single-photon transport from one waveguide to the other. However, strong atom–light interaction can be switched on optically. By ramping the control laser power down to zero, we can store a weak gate pulse inside the atom to drive the atom in state $|g\rangle$. Dipole-induced transmission at the single-photon level causes reciprocal single-photon transport between the two waveguides. The strong atom–light interaction can be turned off by adiabatically reapplying the control beam to drive the atom back to state $|s\rangle$. Incidentally, the bit error rate.[38] of this single-photon interconnection can be estimated by $1-p_{\rm t}$ when the nanowire–waveguide coupling is phase-matched. Assuming $\omega_0=\omega_{\rm at}$, the bit error rates are 22.6% and 10.7% when $P=20$ and 37, respectively. Thus, it is feasible to fabricate such all-optical single-photon interconnectors using current technology.

4. Conclusion

Finally, we come to our conclusion. We have introduced a universal single-photon interconnector composed of two individual nano-waveguides and an optical emitter. Because of the strong coupling between waveguide modes and the emitter, dipole-induced transmission permits reciprocal single-photon transport between two terminal waveguides. In the future, this could be used to realize an efficient and convenient optically controlled interconnector that connects two individual optical nano-devices to a realistic optical circuit. Furthermore, the interconnector is viable not only for single-photon input, but also for multiphoton queue input when the photons are separated by an appropriate distance in the real space.

References

[1] Monroe D 2014 *Commun. ACM* **57** 13
[2] Kim N C, Ko M C and Choe C I 2015 *Plasmonics* **10** 1447
[3] Shen H Z, Zhou Y H and Yi X X 2014 *Phys. Rev. A* **90** 023849
[4] Shen Y, Bradford M and Shen J T 2011 *Phys. Rev. Lett.* **107** 173902
[5] Pepino R A, Cooper J, Anderson D Z and Holland M J 2009 *Phys. Rev. Lett.* **103** 140405
[6] Tiarks D, Baur S, Schneider K, Dürr S and Rempe G 2014 *Phys. Rev. Lett.* **113** 053602
[7] Manzoni M T, Reiter F, Taylor J M and Sørensen A S 2014 *Phys. Rev. B* **89** 180502
[8] Neumeier L, Leib M and Hartmann M J 2013 *Phys. Rev. Lett.* **111** 063601
[9] Chen W, Beck K M, Buecker R, Gullans M, Lukin M D, Tanji-Suzuki H and Vuletic V 2013 *Science* **341** 768
[10] Chang D E, Sorensen A S, Demler E A and Lukin M D 2007 *Nat. Phys.* **3** 807
[11] Birnbaum K M, Boca A, Miller R, Boozer A D, Northup T E and Kimble H J 2005 *Nature* **436** 87
[12] Kuhlmann A V, Prechtel J H, Houel J, Ludwig A, Reuter D, Wieck A D and Warburton R J 2015 *Nat. Commun.* **6** 8204
[13] Ballarini D, De Giorgi M, Cancellieri E, Houdré R, Giacobino E, Cingolani R, Bramati A, Gigli G and Sanvitto D 2013 *Nat. Commun.* **4** 1778
[14] Zhang S, Liu C, Zhou S, Chuu C S, Loy M and Du S 2012 *Phys. Rev. Lett.* **109** 263601
[15] Zhu W, Xiao X, Zhou D L and Zhang P 2016 *Chin. Phys. B* **25** 235
[16] Shen J T and Fan S 2009 *Phys. Rev. A* **79** 023837
[17] Shen J T and Fan S 2009 *Phys. Rev. A* **79** 023838
[18] Shen J T and Fan S 2005 *Opt. Lett.* **30** 2001
[19] Lian T L, Feng J S, Xu W B and Wang B 2014 *Chin. Phys. B* **23** 24202
[20] Wang D, Wu J Z and Zhang J X 2016 *Chin. Phys. B* **25** 230
[21] Gu M, Kang L, Zhao Q Y, Jia T, Wan C, Xu R Y, Yang X Z, Wu P H, Zhang Y and Xia J S 2015 *Chin. Phys. B* **24** 68501
[22] Chen Y, Wubs M, Mørk J and Koenderink A F 2011 *New J. Phys.* **13** 103010
[23] Le Kien F and Rauschenbeutel A 2016 *Phys. Rev.* **A** 93
[24] Mu-Tian C, Gen-Long Y, Wei-Wei Z, and Xiao-San M 2016 *Chin. Phys. Lett.* **33** 024205
[25] Roulet A, Le H N and Scarani V 2016 *Phys. Rev. A* **93**
[26] Guo X, Li C, Dong J, Liu B, Hu S and He Y 2016 *Chin. Phys. B* **25** 114208
[27] Chen Y, Nielsen T R, Gregersen N, Lodahl P and Mørk J 2010 *Phys. Rev. B* **81** 125431
[28] Chen Y, Gregersen N, Nielsen T R, Mørk J and Lodahl P 2010 *Optics Express* **18** 12489
[29] Duan L M, Kuzmich A and Kimble H J 2003 *Phys. Rev. A* **67** 032305
[30] Abramowitz M, Stegun I and Mcquarrie D A 1966 *Am. J. Phys.* **34** 177
[31] Waks E and Vuckovic J 2006 *Phys. Rev. Lett.* **96** 153601
[32] Englund D, Faraon A, Fushman I, Stoltz N, Petroff P and Vuckovic J 2007 *Nature* **450** 857
[33] Li X, Xie L and Wei L F 2015 *Phys. Rev. A* **92** 063840
[34] Jalas D, Petrov A, Eich M, Freude W, Fan S, Yu Z, Baets R, Popovic M, Melloni A, Joannopoulos J D, Vanwolleghem M, Doerr C R and Renner H 2013 *Nat. Photon.* **7** 579
[35] Xia X, Xu J and Yang Y 2014 *J. Opt. Soc. Am. B* **31** 2175
[36] Xia X, Xu J and Yang Y 2014 *Phys. Rev. A* **90** 043857
[37] Xia X W, Zhang X Q, Xu J P and Yang Y P 2016 *Chin. Phys. B* **25**
[38] Chau H F 2002 *Phys. Rev. A* **66** 317